



HAL
open science

Observations of Elves and Radio Wave Perturbations by Intense Lightning

Maja Tomicic, Olivier Chanrion, Thomas Farges, Janusz Mlynarczyk, Ivana Kolmašová, Serge Soula, Jeff Lapierre, Christoph Köhn, Torsten Neubert

► **To cite this version:**

Maja Tomicic, Olivier Chanrion, Thomas Farges, Janusz Mlynarczyk, Ivana Kolmašová, et al.. Observations of Elves and Radio Wave Perturbations by Intense Lightning. *Journal of Geophysical Research: Atmospheres*, 2023, 128 (10), 10.1029/2022JD036541 . hal-04618521

HAL Id: hal-04618521

<https://hal.science/hal-04618521>

Submitted on 21 Jun 2024

HAL is a multi-disciplinary open access archive for the deposit and dissemination of scientific research documents, whether they are published or not. The documents may come from teaching and research institutions in France or abroad, or from public or private research centers.

L'archive ouverte pluridisciplinaire **HAL**, est destinée au dépôt et à la diffusion de documents scientifiques de niveau recherche, publiés ou non, émanant des établissements d'enseignement et de recherche français ou étrangers, des laboratoires publics ou privés.



Distributed under a Creative Commons Attribution - NonCommercial 4.0 International License



RESEARCH ARTICLE

10.1029/2022JD036541

Observations of Elves and Radio Wave Perturbations by Intense Lightning

Key Points:

- Transient luminous events, lightning, and MF and VLF signal perturbations from a thunderstorm system in the Adriatic Sea are analyzed
- 63 elves are observed, with 14 associated LOREs. No sprites or halos
- Several early VLF perturbations caused by either +/-CG or IC lightning discharges are found to not be accompanied by any TLE type

Maja Tomicic¹ , Olivier Chanrion¹ , Thomas Farges² , Janusz Mlynarczyk³ , Ivana Kolmašová^{4,5}, Serge Soula⁶ , Jeff Lapierre⁷, Christoph Köhn¹ , and Torsten Neubert¹ 

¹DTU Space, Technical University of Denmark, Lyngby, Denmark, ²CEA, DAM, DIF, Arpajon, France, ³Institute of Electronics, AGH University of Science and Technology, Krakow, Poland, ⁴Department of Space Physics, Institute of Atmospheric Physics, Czech Academy of Sciences, Prague, Czech Republic, ⁵Faculty of Mathematics and Physics, Charles University, Prague, Czech Republic, ⁶Laboratoire d'Aérodynamique, Université de Toulouse, UT3, CNRS, IRD, Toulouse, France, ⁷Earth Networks, Germantown, MD, USA

Supporting Information:

Supporting Information may be found in the online version of this article.

Correspondence to:

M. Tomicic,
majtom@space.dtu.dk

Citation:

Tomicic, M., Chanrion, O., Farges, T., Mlynarczyk, J., Kolmašová, I., Soula, S., et al. (2023). Observations of elves and radio wave perturbations by intense lightning. *Journal of Geophysical Research: Atmospheres*, 128, e2022JD036541. <https://doi.org/10.1029/2022JD036541>

Received 21 JAN 2022

Accepted 7 APR 2023

Abstract Electromagnetic pulses (EMPs) and quasi-static electric fields (QE) from powerful lightning heat and ionize the lower ionosphere. The EMP disturbance may appear as an elve at ~80–95 km altitude, and the QE field as a halo or a sprite at ~60–80 km altitude. Both are thought to perturb crossing radio signals because of changes to the electrical conductivity of the regions. Here we present an analysis of 63 elves and corresponding radio signal perturbations from an almost stationary thunderstorm system that allows us to untangle some of the dependencies of perturbations on the lightning characteristics. The amplitude perturbations of a VLF-transmitter signal are characterized as either long-recovery, early events (LOREs) or as early events. We find that LOREs are related to lightning with high peak currents and bright elves, and that their sign (amplitude increase or decrease) depends on the relative locations of the transmitter, disturbance and receiver. Based on a subset of strokes, lightning with elves has on average ~3 times the impulse charge-moment-change and power in broadband as lightning of similar peak currents without elves. The early events occur without observed elves, sprites or halos. They recover in ~10–100 s and are observed for both polarities of cloud-to-ground lightning and for intracloud flashes. It is proposed that these observations may relate to regions of reduced conductivity caused by an electron attachment/detachment process at lower heights, or by electron enhancements associated with TLEs that are too dim to be detected by the camera.

Plain Language Summary Powerful lightning can create local disturbances to the atmosphere at around 70–100 km altitude. They appear as optical phenomena known as halos, sprites and elves and as changes in phase and amplitude of radio signals that pass through the disturbed region. The characteristics of the lightning strokes leading to the various types of perturbations are not fully understood. In this work, we analyze 63 elves and corresponding amplitude changes in radio signals from an almost stationary thunderstorm system that allows us to untangle some of the dependencies of perturbations on the lightning characteristics. We find that lightning that produce elves has three times the power and impulse charge moment change than lightning of similar peak current without elves. Also we find that elves are associated with the longest types of perturbations (~10 min duration) in the 3–30 kHz radio signals, whereas the shorter types of perturbations (~1 min duration) appear to be without optical emission. We propose that these observations may relate to regions of reduced conductivity caused by electron attachment/detachment processes at lower heights, or by electron enhancements associated with TLEs that are too dim to be detected by the camera.

1. Introduction

Elves are optical emissions at the base of the ionosphere (~80–95 km altitude) that expand rapidly up to ~700 km diameter during ~1 ms following a powerful cloud-to-ground (CG) lightning stroke. They are emissions from atmospheric constituents that are excited and ionized by collisions with free electrons heated by the electromagnetic pulse (EMP) radiated by the lightning return current (Barrington-Leigh & Inan, 1999; Fukunishi et al., 1996; Van der Velde & Montanyà, 2016). Since their first discovery from the space shuttle orbiters (Boeck et al., 1992), elves have been studied from the ground (e.g., Blaes et al., 2016; Fukunishi et al., 1996; Kolmašová et al., 2021; Van der Velde & Montanyà, 2016), from space (e.g., Chen et al., 2008, 2014; Frey et al., 2005), and with models (e.g., Inan, Sampson, & Taranenko, 1996; Marshall, 2012; Marshall et al., 2010). The properties of lightning return strokes that control the excitation of elve emissions are still not fully understood because comprehensive

© 2023 The Authors.

This is an open access article under the terms of the [Creative Commons Attribution-NonCommercial License](https://creativecommons.org/licenses/by-nc/4.0/), which permits use, distribution and reproduction in any medium, provided the original work is properly cited and is not used for commercial purposes.

data are lacking caused, for instance, by limitations in instrument sensor sensitivities, triggered data selection, and the relatively modest number of optical observations of elves (e.g., Chang et al., 2014; Frey et al., 2005; Lu, 2006). Whereas the radiated EMP power is proportional to the time derivative of the peak current, the most commonly adopted parameter for elve probability is the peak current itself because it is a parameter provided by lightning detection networks. An estimate of the lower limit required to generate elves ranges from ~38 kA (Chen et al., 2014), where elves were observed with the ISUAL spectrophotometer from space, to ~130 kA (Van der Velde & Montanyà, 2016) based on camera observations from ground in Spain and France. Observations in the western United States concluded that the threshold for 50% probability of elves was 88 kA and 90% probability at 106 kA (Blaes et al., 2016). Variations in the altitude of the bottom part of the ionosphere (Han & Cummer, 2010) or in the electron density profile sharpness at the bottom of the ionosphere (Han et al., 2011), may influence the production of elves, as well as meteorological variations such as thunderstorm altitudes, and thereby the average lightning channel length (Blaes et al., 2016). Thus, Van der Velde and Montanyà (2016) found elves far more likely in maritime winter thunderstorms than summer thunderstorms over land and Chen et al. (2014) found only dependence on stroke energy, but no significant oceanic and land difference. The diversity of conditions in the above reports points to the difficulty in determining a globally and seasonally independent lower limit on peak current (or other lightning parameters) for lightning causing elves.

Narrow-band navigational transmitter signals in the VLF band propagate in the Earth-ionosphere wave-guide. They are reflected at elve-altitudes and the signal properties are therefore affected by conductivity changes in this region. The electron density changes associated with elves (Marshall et al., 2010) cause step-like perturbations to the transmitter signals (amplitude and phase) if the transmitter-receiver (TR) path crosses the region affected by the elve. Such perturbations are called Long Recovery Early Events (LOREs) (e.g., Cotts & Inan, 2007; Haldoupis et al., 2013; Mika et al., 2006; NaitAmor et al., 2013; Salut et al., 2012). They fall into the category of early VLF events because they are caused by direct coupling of the lightning EMP and the ionosphere, thus show a very short delay (a few ms) from the return stroke pulse. LOREs persist for tens of minutes, and sometimes the signal does not recover before it is masked by other variations in the signal levels (Cotts & Inan, 2007; Mika et al., 2006). The long recovery time is linked to the lifetime of free electrons at this altitude (Gordillo-Vázquez et al., 2016; Rodger, 2003). The LORE phenomenon has almost exclusively been observed in association with elves and is considered the VLF signature of elves (Haldoupis et al., 2012, 2013; Kolmašová et al., 2021), although data sets with more than eight elve-LORE pairs from the same instruments have not been published until now.

On the other hand, the physical mechanisms responsible for early/fast and early/slow VLF events (Haldoupis et al., 2006, 2009; Inan et al., 1993, 2010), which are similar to LOREs but with recovery within a few minutes, are still under debate (Kabirzadeh et al., 2017; Marshall et al., 2008). The relatively fast recovery suggests they are caused by perturbations to the conductivity at lower altitudes where the lifetimes of free electrons are of the order of 10–100 s (Haldoupis et al., 2009; Pasko & Inan, 1994; Rodger et al., 1998). Consistent with this, they have been found to relate to sprites (Haldoupis et al., 2004, 2010; Inan et al., 1995) and sprite halos (Moore et al., 2003) in the mesosphere. However, observations of early/fast events with no apparent luminous emissions have also been reported (Marshall et al., 2006), as have events that appear related to elves (Mika et al., 2006).

Narrow band radio emissions in the Medium Frequency (MF) range (0.3–3 MHz) are mainly amplitude modulated and propagate over long distances during the nighttime by reflection on the E-region of the ionosphere at ~105 km. During the day, when the altitude of reflection is lower, the interaction with a denser atmosphere leads to strong absorption that can induce attenuation of the wave amplitude of more than two orders of magnitude. In contrast, during the night, the amplitude of the MF waves is rather constant (Davies, 1990). Carpenter et al. (1984) found disturbances at 780 kHz on an 1,800 km link with a maximum amplitude of 3 dB. According to Carpenter et al. (1984), these disturbances develop much faster than the disturbances typically observed in this frequency band and last a few tens of seconds. The explanation is the electrons that precipitate into the lower ionosphere (85 km) within range of the radio link induced by whistlers produced by lightning in the opposite hemisphere. Using broadband measurements, Farges et al. (2007) observed, for the first time to the authors' knowledge, the effects of lightning on MF radio emissions when thunderstorms occur between the transmitters and the receiver. During the summer of 2004, Farges et al. (2007) analyzed the broadband signals recorded from more than 4,000 nighttime lightning events. The manual analysis of the waveforms, extracted by narrow-band filtering around nine MF transmission frequencies between 800 and 1,600 kHz, shows the existence of disturbances of very short duration (a few milliseconds) but of high amplitude (10–15 dB). The amplitude of the disturbance is found to be related to the peak current of the CG stroke (see their Figure 3). Depending on the amplitude of the peak current, between 1 and 5 MF radio links are

simultaneously impacted (see their Figure 5), showing that the propagation disturbance phenomenon has an horizontal extension of 200–300 km in radius (see their Figure 10). A statistical analysis of the main elements describing the shape of the disturbances (amplitude, duration, rise time, etc.) observed on nine MF radio links is provided in Farges et al. (2007). To understand this brief attenuation phenomenon, Farges et al. (2007) modeled the propagation of the MF radio waves through a region of the ionosphere disturbed by the lightning EMP under three different scenarios: that the EMP causes only ionization, only electron heating, and both combined. The results were compared to the absorption calculations obtained in the absence of lightning and showed that electron heating alone could explain the measured attenuation (see their Figure 13). Moreover, the decay of electron heating, which is less than 100 ms at elve altitudes (Rodger et al., 1998), is the only process that is compatible with the observed attenuation (1–10 ms). For comparison, the decay of enhanced ionization is 10,000 times longer, when observed with narrowband VLF measurements. Finally, Farges et al. (2007) concluded that the disturbances could be an additional signature of the presence of elves. However, simultaneous observations of elves and MF attenuations have not been published until now.

In this paper, we present observations of a high number of elves produced over the Adriatic Sea during the night of 9–10 December 2020, with simultaneous observations of perturbations in the signals of one VLF link and seven MF links passing the region. Our goal is to investigate the relationship between lightning characteristics and lightning effects in the ionosphere. For the first time (to our knowledge), optical observations of 63 elves were recorded from an almost stationary storm. The observations offer a rare opportunity to limit the influence of geographic location, local time and season, viewing conditions and instrument sensitivity while still having a relatively large data sample. We include in our analysis impulse current moment changes (iCMC) and charge moment changes (CMC) of selected strokes derived from Extremely Low Frequency (ELF) measurements and energy of causative strokes from broadband electric field measurements. The relationship between the LOREs of positive and negative polarity is discussed from perturbations by a second storm on the Italian south coast toward the Tyrrhenian Sea.

2. Data, Instrumentation and Methods

2.1. Lightning Data

We use lightning data from the Vaisala Global Lightning Dataset, GLD360 (Said et al., 2010; Said & Murphy, 2016). It contains time, location, peak current and type (CG or intracloud (IC)). The detection efficiency (DE) and location accuracy (LA) for CG flashes in the USA is evaluated to ~75%–85% relative to the National Lightning Detection Network, which has a CG flash DE > 95% (Mallick et al., 2014). The median LA for CG strokes is 1.8 km. The accuracy in the Adriatic Sea is assumed to be the same, since an earlier test in Europe showed better DE and LA than those found in the USA (Poelman et al., 2013). We also use lightning data from The Earth Networks Total Lightning Network (ENTLN) (Lapierre et al., 2019; Zhu et al., 2022). Its CG flash DE and LA in Florida, USA is evaluated to be >98% and 91 m, respectively (Zhu et al., 2022). These parameters vary with network sensor density. For some lightning events, that will be discussed in Section 4.4.2, ENTNL provided the lightning waveforms which were interpreted manually.

2.2. Broadband Electric-Field Sensor

The vertical broadband electric field from 1 kHz to 5 MHz was measured with a dipole whip antenna installed in the center of France (46.1°N, 2.8°E), 882–1,330 km from the storm location (labeled BB in Figure 1). The system is the same as the one presented in Farges and Blanc (2011). It measures the variation of the electric field and triggers if the variation exceeds 2 V/m, storing 30 ms of data from 6 ms before the trigger at a sampling frequency of 12.5 MHz. The resolution is 14 bits and the dynamic range is ± 200 V/m. We use the measurements to characterize lightning and attenuation of MF radio transmitter signals.

2.3. ELF Receiver

The current moment waveform (CMW) and CMC were obtained from measurements of an ELF receiver system in the Bieszczady mountains in Poland (49.2°N, 22.5°E ~850 km from the storm and labeled ELF in Figure 1). It measures the magnetic field component with two antennas aligned in the geographic north-south and east-west directions in the frequency range 0.02 Hz–1.1 kHz. The receiver features a Bessel anti-aliasing filter with a bandwidth of 900 Hz. The sampling frequency is 3 kHz. The CMW and the CMC were reconstructed using the method of Mlynarczyk et al. (2015) that accounts for the dependence with the frequency of the signal attenuation and the propagation velocity in the ELF range.

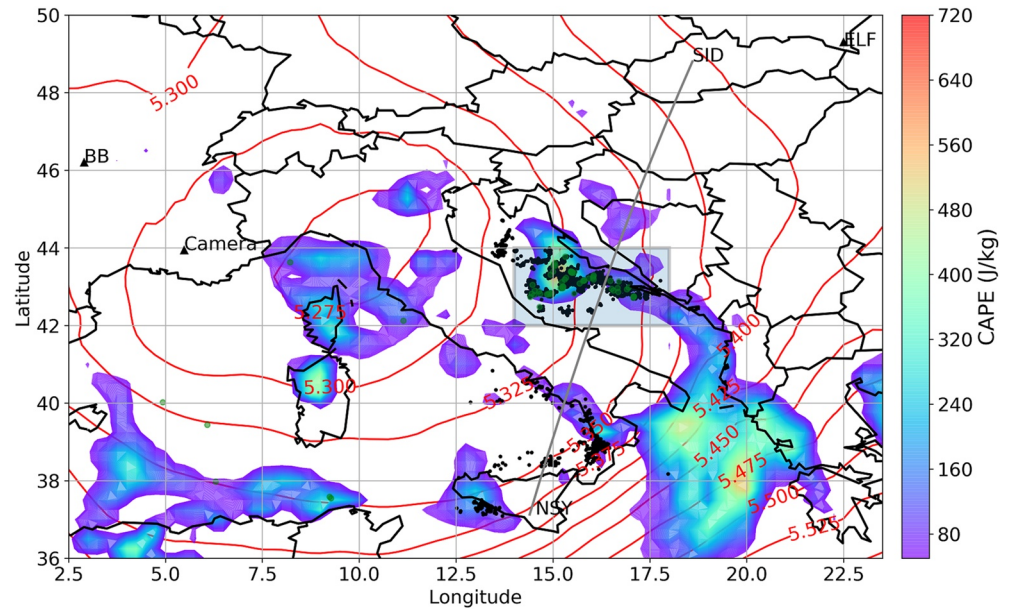


Figure 1. Overview map showing the location of instrumentation used in this study. All CG lightning strokes within ~ 250 km from the GCP of the VLF signal are plotted in black and the elve producing strokes in green. Red contour lines show the geopotential height at 500 hPa and CAPE is shown in colors. The rectangle frames the region where the elves were observed.

2.4. VLF Receiver

A Sudden Ionospheric Disturbances (SID) monitor measures perturbations to narrow-band VLF signals from powerful transmitters used for communication with submarines. The monitor used in this study is operated by the Slovak Organization for Space Activities and placed in Bojnice, Slovakia (48.8°N , 18.6°E , labeled SID in Figure 1). It can record up to 16 VLF transmitters simultaneously with a sampling frequency of 2 Hz. We use the NSY transmitter operated by the Naval Computer and Telecommunications Station in Sicily (37.1°N , 14.4°E), which broadcasts at 45.9 kHz with 250 kW. The signal propagates from Sicily to Slovakia ($\sim 1,345$ km) and reflects multiple times at the surface of the Earth and the bottom of the ionosphere. The propagation great circle path (GCP) of the NSY signal crosses directly the thunderstorm location (see Figure 1).

The NSY-SID link is the only VLF link we could identify that passes the thunderstorm area. The analog output of the SID monitor is digitized at a relatively modest rate of 2 Hz because it is designed to detect solar flare effects on the D-region ionosphere. Although the sampling rate is too low for the unambiguous identification of LORES and early/fast, early/slow events, we use the data to identify such events in lack of alternative VLF systems with higher temporal resolution. Ideally, the identification of these events requires accuracy of a few ms to determine their onset time, 20 ms to identify fast events, and 200 ms to distinguish between fast and slow events. It means we cannot distinguish between early/fast and early/slow, but lump the two into “early” events. We then identify perturbations as LORES or “early” if they correlate with CG strokes within the 0.5 s uncertainty of the onset time and otherwise have the same pulse characteristics as such events. As we are not aware of alternative event types that resemble “early” observations, we suggest their identification is quite robust. We note that although the link passes close to the active thunderstorm cells, LORES and early events may be missed because of VLF mode coupling, the properties of the Earth-ionosphere waveguide, or properties of the disturbed region (Haldoupis et al., 2010).

2.5. Optical Observations

The optical observations are performed by a TLE observatory installed in Rustrel, France (43.94°N , 5.48°E) at 1,025 m altitude. It is mounted on a building made available by Laboratoire Souterrain à Bas Bruit (LSBB). The camera is a Watec 1/2” monochrome CCD camera (WAT-902H) with a 16 mm lens that gives 23° horizontal and 17° vertical field of view (FOV). It takes 50 de-interlaced fields per second, corresponding to a time resolution of 20 ms. The images are time referenced after synchronization with an NTP server, giving an absolute time uncer-

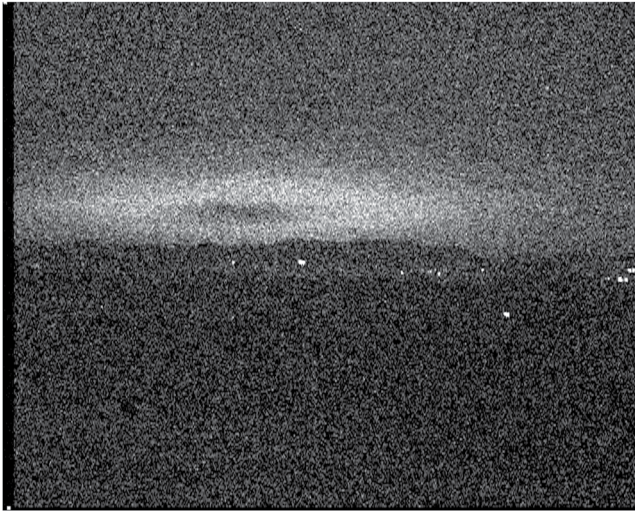


Figure 2. Example of elve image from this study. This elve appeared on 10 December 2020, at 03:57:56.578 UTC.

tainty below 5 ms. The camera is mounted on a QuickSet motorized Pan-Tilt unit allowing for active and automatic tracking of thunderstorms. The night of the observations, the camera tracked two thunderstorms automatically, selecting a new pointing direction every 15 min. The camera, therefore, pointed away from the storm during parts of the night (see Section 4.1 for the gaps). The analysis excludes strokes that occurred in these gaps. From 02:45 UTC the camera stayed in the same position for the rest of the night.

2.5.1. Methods and Error Estimations

Figure 2 shows an image of an elve observed at 03:57:56.578 UTC on 10 December 2020. The rest of the elves are shown in Figures S2–S64 of Supporting Information S1. From the images, we estimated their altitude and relative brightness. Following Van der Velde and Montanya (2016), we calculated the altitude by combining the elevation of the elve centers with the location of the CG stroke reported by GLD360. The elevation angle was retrieved by matching the background stars to the star catalog in the software ‘Cartes du ciel’. The calculations are done assuming a spherical Earth with radius of 6,370 km and a camera altitude of 1,025 m. Before the image analysis, the background for each elve, determined as the mean value of two de-interlaced fields preceding the elve, was subtracted. The elve centers were estimated manually with the cursor. Since the elves are faint and diffuse, their

centers can be difficult to determine, which introduces an error in the elevation angle. Repeated estimates suggest that the uncertainty in this naked-eye method is 0.1° , which corresponds to an altitude uncertainty of ± 1.4 km at 800 km distance to the elves. The uncertainty in the location of the parent strokes (median value 1.8 km (Said & Murphy, 2016)) introduces an uncertainty of around 0.3 km at 800 km distance to the storm. We estimated the relative brightness of the elves from the sum of all pixels in the background-subtracted elve images after dividing by the width of the elve expressed in number of pixels. The brightest elve was used as a reference.

3. Meteorology and Storm Development

On 9 December 2020, a low-pressure system was centered over northern Italy according to the geopotential at 500 hPa with a minimum below 5.275 km (red lines in Figure 1). The counter-clockwise winds reached up to 40 m s^{-1} at 500 hPa (~ 5.5 km), corresponding to large geopotential gradients along an arc extending over northern Africa and southern Italy. This jet carried warm, humid air from the Mediterranean Sea to the Adriatic Sea, enhancing strong atmospheric forcing in the region. Over the Adriatic Sea, the wind shear between 1,000 and 500 hPa (0–5.5 km) was modest, and the CAPE was moderate ($< 700 \text{ J kg}^{-1}$) and higher over water. These conditions led to several electrically active cells that produced lightning with high peak currents. Figure 3 shows the rate and the peak current values of the CG strokes detected in the rectangle displayed in Figure 1 from 19:00 UTC to 06:00 UTC by GLD360 and Figure 4 shows the cloud top temperature (CTT) in the Adriatic Sea region where the elves were observed. The CTT is obtained from the $10.8 \mu\text{m}$ band of the Spinning Enhanced Visible and InfraRed Imager (SEVIRI) on the Meteosat Second Generation (MSG) satellite and is shown here for each hour of elve observation (20:00 UTC to 05:00 UTC). The CTT data is corrected for parallax, corresponding to 0.1° in latitude and 0.03° in longitude for cloud tops at ~ 10 km altitude. All CG strokes with peak currents above 200 kA in absolute value are plotted with black crosses, and the elve-producing strokes are plotted in green. The elve-producing cells are less than 100 km across at $\text{CTT} < -40^\circ\text{C}$ (blue regions in Figure 4). The coldest CTT is about -60°C , which is not much colder than the tropopause (-56°C according to NCEP/NCAR Reanalysis 1) at the same location, suggesting the clouds did not reach much above the tropopause. The elves were caused by strokes over the Adriatic Sea, where CAPE was higher than over land. The CG stroke rate of the Adriatic storm does not exceed 10 strokes per minute, as seen from Figure 3. The relatively low convective activity, seen from the modest development of clouds cells and low stroke rate, is due to the limited CAPE and wind shear over the Adriatic Sea. From GLD360 we also get that 91% of the CG strokes produced in the Adriatic region (gray rectangle in Figure 1) from 19:00 to 6:00 UTC were negative with a high average peak current at -92 kA. The lightning activity and duration of the storm are similar to the storm studied in Chang et al. (2014) which produced 64 observed elves. The elve-producing strokes are shown with green markers in Figure 3 and all had absolute peak currents larger than 228 kA with an average of 453 kA.

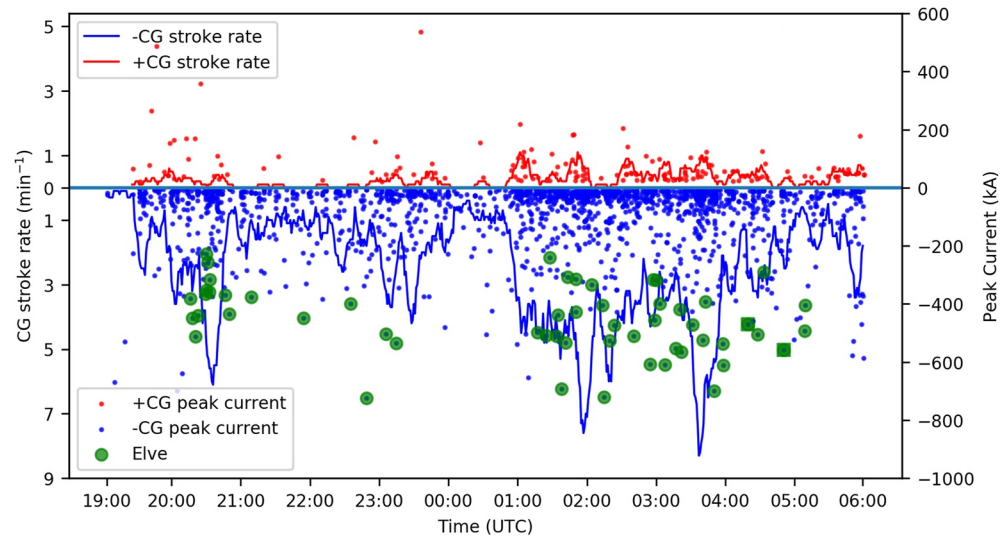


Figure 3. GLD360 data for CG stroke rate and peak current for negative (blue) and positive (red) strokes in the Adriatic Sea on the night of 9–10 December 2020. The green markers show the current of elve producing strokes. We note that the two elve-producing strokes marked with green square markers (at 04:19 and 04:50 UTC), were reported by GLD360 as having positive polarity, but had negative polarity when measured by the ELF antenna.

4. Observations

4.1. Elves

During the night of the storm, the camera in Rustrel detected 63 elves above the Adriatic Sea. One is shown in Figure 2, and the rest in Figures S2–S64 of Supporting Information S1. We note that the large distance, and thereby the low elevation angle, leads to high atmospheric absorption of photons, which reduces the detection efficiency of elves by the camera. In Chang et al. (2010), the ISUAL FUV photometer on the FORMOSAT-2 satellite appeared to detect 16 times more elves than the imager, also suggesting that a large number of events may be below a sensor detection threshold. The lowest altitude at the storm that the camera could observe was 50 km (at 750 km distance) and 80 km (at 950 km distance). These values are calculated using great circle geometry assuming a spherical Earth with radius 6,370 km, a camera altitude at 1,025 m and based on an estimation in “Cartes du Ciel” that the horizon is at around 0.4° of elevation. Thus, we cannot rule out other TLEs, such as sprites and halos, occurring below these altitudes. The camera observed the storm from 20:00 to 05:35 UTC with gaps totaling 1 hour and 45 min (22:00–22:30; 23:30–00:00; 00:30–01:15 UTC).

The optical characteristics were studied for all but a few elves: In four cases, no parent stroke was reported by GLD360 that allowed the estimation of their distance, three were too faint to define their shape, and the brightness of four could not be determined because the moon was behind the elve in the video field. Thus, out of 63 elves, 56 were used for the brightness and altitude calculations.

The altitudes of the elves ranged from 80 to 90 km (see Figure S1 in Supporting Information S1), which is within the range and variability of the results in Van der Velde and Montanyà (2016). All elves below 83 km occurred in the first hour of observations. We attribute this to the storm itself and not to changes in the ionosphere based on results from the NASA international reference ionosphere model (IRI) that appear to be constant. There is no clear trend between altitude and local time for the rest of the night, as seen from the altitude versus time plot in Figure S1 of Supporting Information S1. The relative brightness varies down to ~17% of the brightest elve. The brightness is correlated with the peak current and the Power Spectral Density (PSD) of the parent stroke in the band of the broadband receiver (see below), a parameter discussed in later paragraphs.

4.2. Lightning Broadband Waveforms

During the periods the camera observed the storm, GLD360 detected 234 CG strokes with absolute peak current values above 200 kA within the camera's FOV. This means that 63 strokes produced elves and 175 strokes did not produce observable elves (four elves did not have matching strokes). To understand why some produce elves and

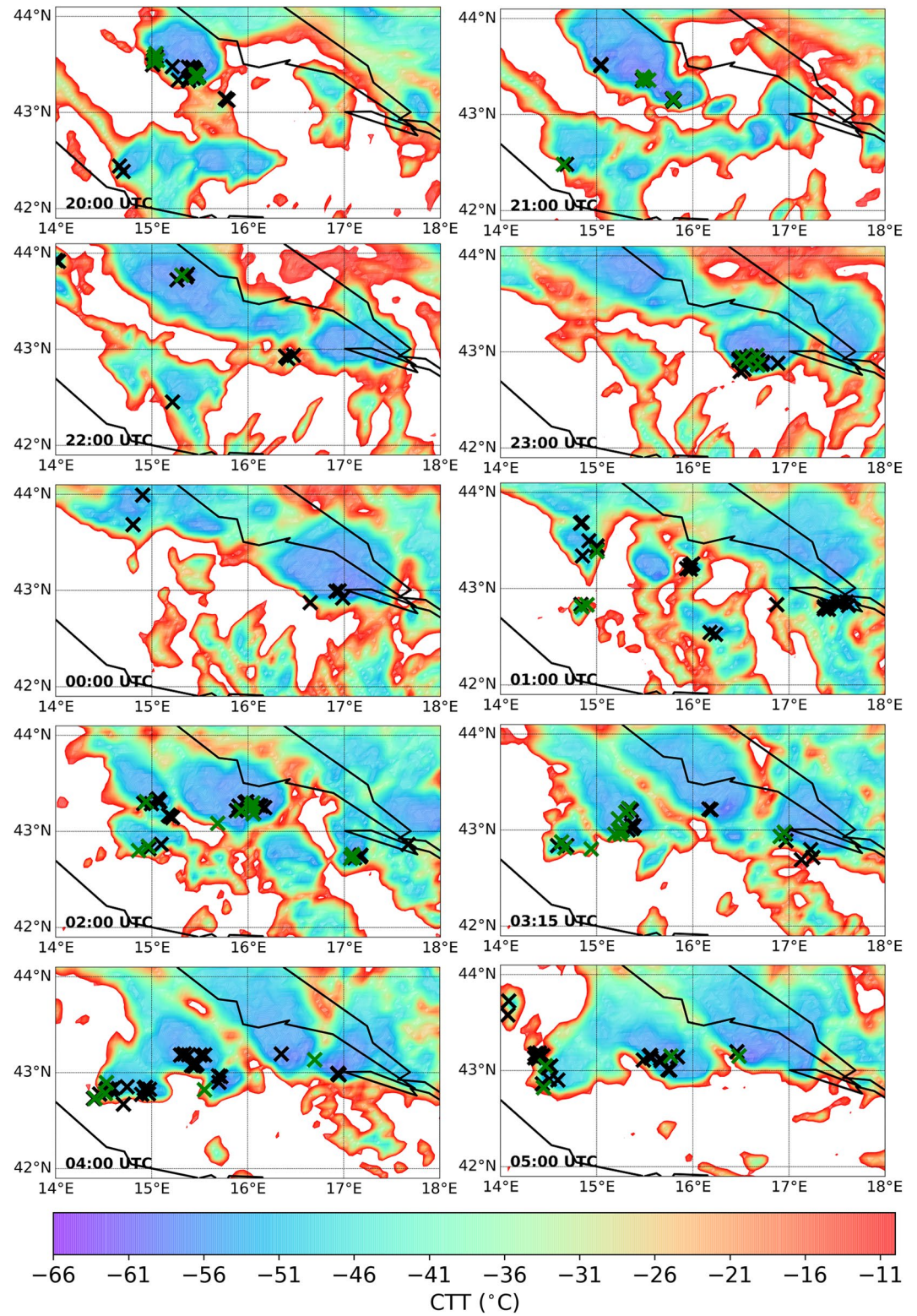


Figure 4. Hourly snapshots of cloud top temperature (CTT). Strokes with peak currents absolute values higher than 200 kA marked with black crosses from 20 to 05 UTC. The elve-producing strokes are plotted in green.

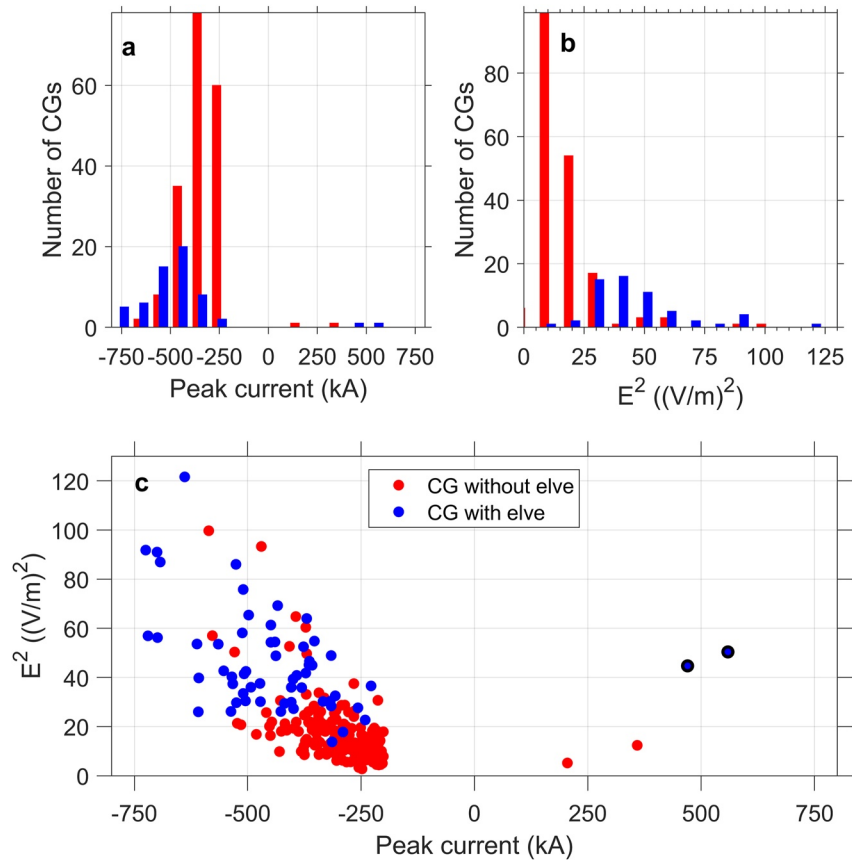


Figure 5. (a) Peak current as reported by GLD360. CG strokes with peak current above 200 kA that did and did not produce observable elves are shown in blue and red respectively. We note that the two elve producing positive CG strokes (marked with black), were of negative polarity when measured with the ELF antenna. (b) The E^2 of the electric field in the band from 1 kHz to 5 MHz computed over 1.5 ms from the arrival time of the ground wave. (c) E^2 as a function of peak current.

others do not, we analyzed the waveform of the vertical electric field from the lightning strokes, measured by the broadband receiver in France. For each stroke, we determined the maximum amplitude of the ground wave (E_{GW}), the rise-time of the electric field pulse, defined as the time from 50% to 90% of E_{GW} , and the fall time from the maximum to the background. The statistics, presented in Table S2 of Supporting Information S1, show no apparent difference between strokes with and without elves. Comparing the average of the normalized electric field waveforms of strokes with and without elves (Figure S66 in Supporting Information S1) shows that the ground wave and the first sky wave on average have similar amplitudes, and that the second sky wave and the following ones (third and fourth) are stronger with elves.

In Blaes et al. (2016), the peak current of the CG stroke is found to be a decisive parameter for elve generation, with a probability reaching 50% at 88 kA. Other authors found thresholds from 38 to 130 kA (Chen et al., 2014; Van der Velde & Montanyà, 2016). In our case, the formation threshold of elves is around 200 kA. The variability of reported thresholds is likely an effect of the sensitivity of the optical instrument used (camera or photometer, e.g.), or uncertainty in the estimation of the peak currents reported by the detection networks. However, a question remains why not all high-current strokes generate bright elves, as noted in Kolmašová et al. (2021).

To explore this question further, we computed the electric field wave power, E^2 , which is the frequency integral of the electric field PSD over the whole antenna bandwidth (1 kHz–5 MHz) using the method of Ripoll et al. (2021). It is computed over 1.5 ms from the arrival time of the ground wave, to include the ground wave and all the sky waves. Figure 5 shows that the CG strokes producing observable elves have on average 3.23 larger power than those that did not. We also see from Table S2 in Supporting Information S1 that the elve producing strokes in this study have three orders of magnitude (1593X) larger power than the typical flashes analyzed in

Table 1
Comparison of Impulse Charge Moment Change (iCMC) and Maximum Current Moment (CM) for Strokes That Produced Elves (E), Elves and LOREs (E + L) or Not (No E)

Event	Time (UTC)	Lon (deg)	Lat (deg)	Peak current (kA)	iCMC (C km)	CM (kA km)
E + L	12-09 20:09:08.217	15.46	43.39	-639	-133.2	-122
E + L	12-09 22:48:54.353	16.56	42.90	-725	-148.5	-146
E + L	12-10 01:33:38.668	15.68	43.09	-520	-146.6	-137
E + L	12-09 23:05:50.076	16.67	42.97	-504	-106.5	-93
E	12-09 23:14:30.984	16.68	42.87	-535	-134.0	-120
E	12-10 01:16:58.561	14.84	42.81	-498	-117.4	-108
No E	12-09 20:25:15.397	15.27	43.34	+359 ^a	-59.1	-55
No E	12-10 01:41:08.681	18.54	42.51	-430	-29.3	-33
No E	12-10 02:33:11.310	18.45	42.66	-378	-32.7	-30
No E	12-10 03:31:06.092	14.74	42.85	-426	-43.8	-39

^aReported polarities disagree.

Ripoll et al. (2021) using the same electric field sensor. This suggests that the generation of elves depends on the complete electromagnetic energy release of the stroke.

4.3. ELF Measurements

We analyzed ELF measurements of the electromagnetic signals from a subset of the lightning strokes by the sensor in the Bieszczady Mountains in Poland. The selection included high-current strokes with and without elves, and strokes with elves associated with LOREs and not. The selection was made to use events that occurred at different times throughout the night. We calculated the current moment (CM) and the impulse charge moment change (iCMC) (Cummer & Lyons, 2004) defined as the total CMC during the first 2 ms of the lightning stroke according to the method of Mlynarczyk et al. (2015). The iCMC is likely more relevant for elves than the total CMC since elves are generated within the first milliseconds. The results and other relevant stroke parameters are presented in Table 1. The average iCMC is -131 ± 16.4 C km for strokes that generate elves and -41.2 ± 13.4 C km for strokes without observable elves. The average maximum CM is -121 ± 19.2 kA km and -39.25 ± 11.1 kA km for the two types, respectively. Thus, in this sample, the average iCMC is 3.1 times larger and the average maximum CM is 3.2 times larger for strokes that generate elves. Larger values can result from

larger currents, longer channel lengths, or both. Since GLD360 data only provide the maximum current obtained in the VLF range, one cannot expect full correlation with the iCMC or CM, as pointed out in Lu et al. (2012). Large iCMC values are closely related to sprite and halo production. However, since the elves, for which we calculated the iCMC, were all caused by -CG lightning and the common threshold for sprite productions is around 600 C km (Cummer & Lyons, 2005) and possibly higher for negative sprites (e.g., Qin et al., 2013), we do not find it likely that there were elve-sprite pairs in these cases. In addition, the camera would most likely observe halos or sprites, had they been there. One must think more, however, as to what the physical significance of the large CMs and iCMCs is, in relation to lightning that causes bright elves. This would require modeling and could be the topic of a new paper. Their relation to LOREs is discussed in a following paragraph.

4.4. VLF Transmitter Signal Perturbations

The amplitude of the NSY VLF signal from the night of 9–10 December is shown in Figure 6 on different temporal scales. The variation on scales larger than ~30 min are not related to thunderstorm activity, but to other ionospheric processes (e.g., Hunsucker (1982); Kumar et al. (2017) and references therein) because the signal from the same transmitter during a night without storms shows similar variations. However, amplitude perturbations on shorter scales are multiple, and many correlate in time with lightning activity detected by GLD360. These are identified using the criterion that the perturbation amplitude must be greater than 0.25 dB relative to the average amplitude (in dB) of the preceding 10 s. This condition corresponds to a threshold of 4σ , where σ is the average standard deviation for the night. The value is close to the typical value at 0.2 dB of Inan, Pasko, and Bell (1996). In addition, we require a lightning stroke to be detected by GLD360, or an elve by the camera, within 0.5 s before the perturbation. The 0.5 s limit corresponds to the temporal resolution of the receiver. The algorithm used to identify candidate events is used on a 3-point moving average of the signal, shown in Figure 6 in red. All candidate events are manually validated and categorized.

The time resolution of the VLF receiver allows for classification in LOREs and early events, but not distinction between early/fast and early/slow events (Section 2.4), and is sufficient to exclude most lightning-induced electron precipitation events that have onsets 0.3–1.6 s relative to their causative stroke (Burgess, 1993; Peter & Inan, 2007). The two types are identified using a 20-point moving average (corresponding to 10 s), and are shown in Figures 6 and 7. Early events appear as sudden increases in the signal with a recovery (decrease of signal) that starts within 10 s after the peak. These events, therefore, appear as a peak with no plateau on the top in the smoothed signal. In our signal, we categorize LOREs as step-like perturbations that can be either positive or negative and that do not show recovery within the first 20 s. It means there will be either a plateau after the

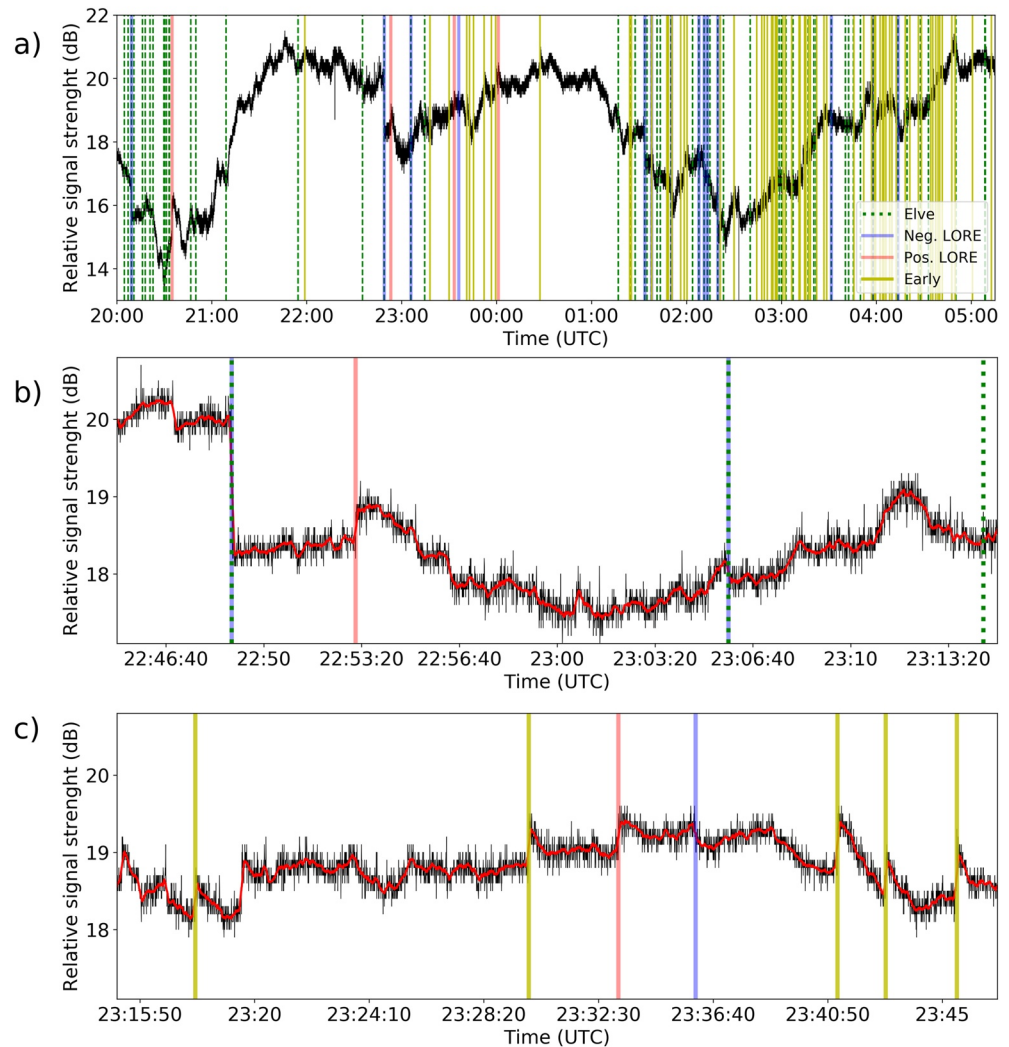


Figure 6. (a) Intensity of the NSY VLF signal (45.9 kHz) recorded in Bojnice (Slovakia) on the night of 9–10 December 2020. Overlaid are the times of elves, LOREs and early events. (b) A zoom of the signal in the time 22:45–23:15 UTC. (c) A zoom of the signal in the time 23:15–23:47 UTC.

step or the amplitude keeps decreasing/increasing for at least 20 s (see the example in Figure 7a). We identify 68 early events (all with positive amplitude) and 18 LOREs (14 negative and 4 positive). The events are marked in Figure 6 and the main characteristics of the lightning strokes related to the two types of perturbations are given in Table 2. There are also signal perturbations related to high peak current lightning or even elves that have the shape of negative amplitude LOREs except that the onset is significantly slower at 1–3 s. One example is seen in Figure 6b at 22:46:53 UTC. For brevity, such events are not investigated further in this work.

Because of the considerable variation of the background signal and the high number of lightning-induced perturbations, it is hard to determine a recovery time for the individual perturbations. However, for all the early events, the recovery time looks shorter than 3 min (most are ~ 1 min), which is consistent with the typical recovery time of these events of 10–100 s (Inan et al., 2010; Inan, Pasko, & Bell, 1996). The LOREs may not recover before other variations mask them. However, they appear longer than the early events. In some cases, the perturbation is hard to categorize (positive LORE or early event) because the LORE step or the shape of an early event is unclear due to the varying background signal. Another complication is that perturbations can overlap. Thus, a few events can be miscategorized.

Figures 8a and 8c show the location of the lightning strokes related to the different types of perturbation and Figure 8b a histogram of the minimum distance from the stroke to the VLF path for LOREs and early events.

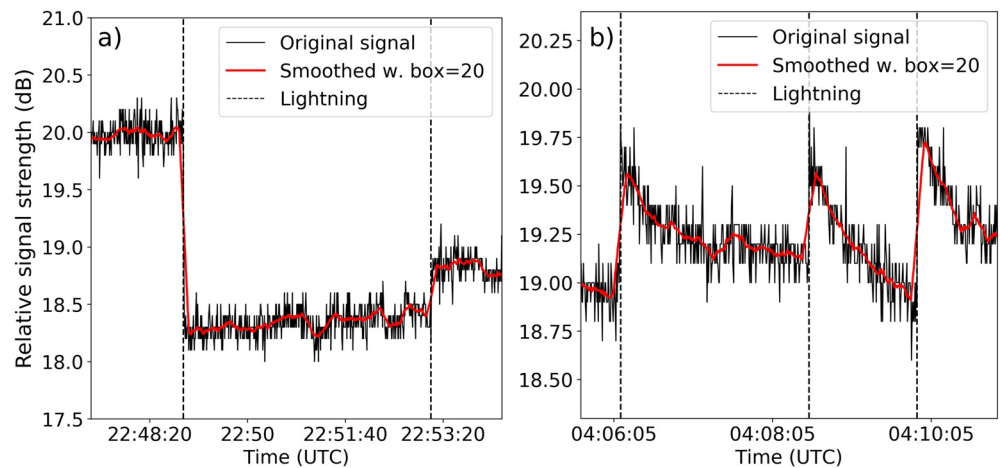


Figure 7. (a) An example of a negative and positive LORE event. The negative LORE is caused by a lightning stroke of -725 kA that also produced an elfe. The positive LORE is caused by a 530 kA stroke which would likely produce an elfe, but the camera was not pointed toward its direction. (b) Three examples of early events. The first and third have simultaneous strokes with -121 kA and $+59$ kA currents. The second has no identified stroke but coincides with an IC pulse of -7 kA.

4.4.1. LOREs

All but one of the 14 negative LOREs were associated with elves caused by lightning strokes of peak current ranging from 314 to 725 kA. The remaining negative LORE (at 23:36 UTC) occurred simultaneously with a lightning stroke with a peak current of $+536$ kA when the camera was not observing the storm. Thus, it is likely that there was an elfe at the time. These results show that the perturbations considered as LOREs are related to elves. The four positive LOREs were generated by the storm on the south-west coast of Italy, not covered by the camera. However, the related lightning strokes had high peak currents, ranging from -383 kA to -631 kA, making them very likely to produce elves (Kolmašová et al., 2021). In agreement with previous studies based on observations and modeling (Haldoupis et al., 2013; Marshall & Inan, 2010; Naitamor et al., 2013), the decrease or increase in the signal amplitudes is a signal propagation effect that depends on the relative locations of the transmitter, disturbance, and receiver. As seen from Figure 6a, most of the recorded elves (78%) were not associated with perturbations in the VLF signal, although they were caused by very high peak current lightning and occurred within 150 km from the VLF link. This observation will be discussed in Section 5.

4.4.2. Early VLF Events

The early events, all seen as increases in the VLF signal, are unrelated to elves but correlate in time with lightning of both polarities within 150 km of the VLF path. The median of the absolute values of peak currents is 45 kA and, as seen from Table 2, much lower than for the LORE-producing strokes. The mean peak current and 95% confidence interval calculated for the early event strokes match the peak current intensities reported for this type of phenomenon earlier, for example, 20–180 kA in Inan, Pasko, and Bell (1996).

Nineteen early events were associated with IC discharges with peak currents between 3 and 42 kA, as measured by GLD360. ENTNLN reported 12 of these as IC discharges, 4 as CG strokes (with low currents 5–8 kA) and 3 were undetected. Inspection of the ENTNLN waveform data found no sign of CG strokes for the events that were labeled as IC pulses that could have been missed by the detection algorithm. This suggests that at least some early events were caused by IC lightning. The location of the IC discharges is marked by cyan stars in Figure 8c.

4.5. MF Radio Wave Attenuation

As mentioned in the introduction, Farges et al. (2007) conducted a statistical analysis of MF attenuation related to more than 4,000 nighttime CG strokes

Table 2
Statistics From GLD360 Data on the Two Types of VLF Perturbations

	LORE	Early
# of events (pos/neg amplitude)	18 (4/14)	68 (68/0)
Lightning peak current parameters in absolute value		
Range (kA) [min max]	[314,725]	[3 660]
# CG/IC	15/0 ^a	49/19
# Neg/pos CG	14/1 ^a	28/21
# Neg/pos IC	0/0 ^a	2/17
Mean/Median (kA)	526/526	82/45
95% conf. int. (kA)	[461,592]	[55,108]

^aThree events do not have parent lightning detected by GLD360, but coincide with elves.

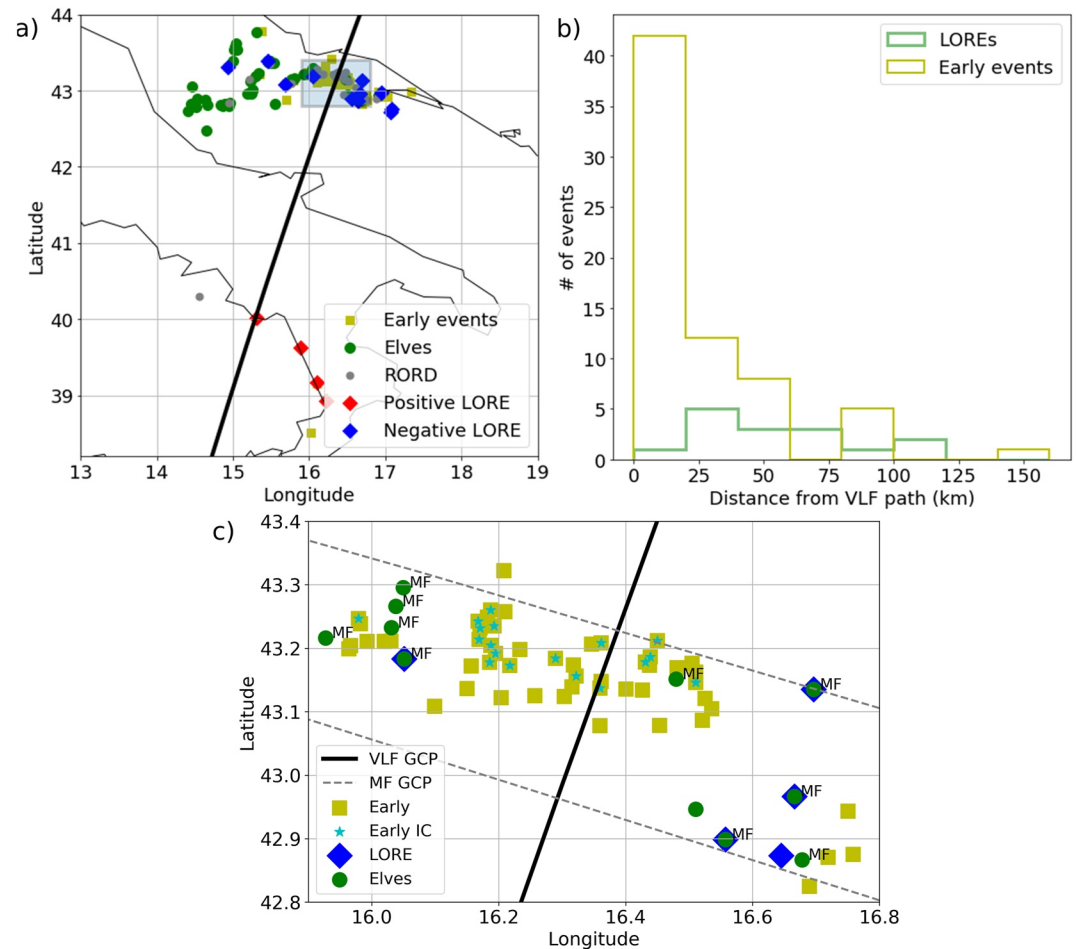


Figure 8. (a) Locations of elve-producing strokes (green dots) and LORE-producing strokes (blue/red diamonds). The lightning responsible for early events are shown with yellow squares. The VLF GCP is shown in black. (b) Histogram showing the distance between causative lightning stroke and VLF GCP for the two types of events. (c) Zoom to the region marked with a rectangle in panel (a). In addition to the markers in panel (a), we highlight the early events produced by IC pulses with cyan stars and annotate MF attenuations related to an elve. Gray dashed lines are MF GCPs that cross this region.

with peak currents from 10 kA to more than 100 kA. They used nine radio links between 900 and 1,557 kHz with the transmitters located between 380 and 970 km from the receiver. They found that the temporal variation of the MF attenuation matches the typical rise time and duration of optical pulses of elves and that MF-attenuation can be detected for lightning to a distance from the ray-path that compares to the radii of elves (Farges et al., 2007). This suggests a fast process in elve regions, which led Farges et al. (2007) to conclude that attenuation was caused by electronic heating of the lower ionosphere by the EMP.

Here we explore the impact of CG strokes with an absolute peak current value greater than 200 kA, some of which triggered observable elves. Our objective is to know how the elve presence contributes to the occurrence of the MF perturbations. During the storm of 9–10 December 2020, 59 out of 234 CG strokes with peak current above 200 kA were followed by the observation of an elve. For this study, we use exactly the same method of data analysis as Farges et al. (2007), whose main steps are recalled in the Supporting Information for easier reading. The new results presented here can thus be fully compared to those of Farges et al. (2007).

We identified seven MF radio transmitters from www.mwlist.org, where the signals to the receiver pass over the storm. More information about the MF transmitters is provided in Table S1 of Supporting Information S1. An example of an MF perturbation when an elve occurs is shown in Figure 9. The top panel shows the broadband waveform corresponding to the –CG stroke that was associated with an elve at 03:57:56.578 UTC, the middle panel shows the corresponding narrow-band signal amplitudes of four MF transmitters at 540 kHz, 576 kHz, 630 kHz, and 891 kHz, and the bottom panel shows the GCPs of the signals TR path. The attenuation is most

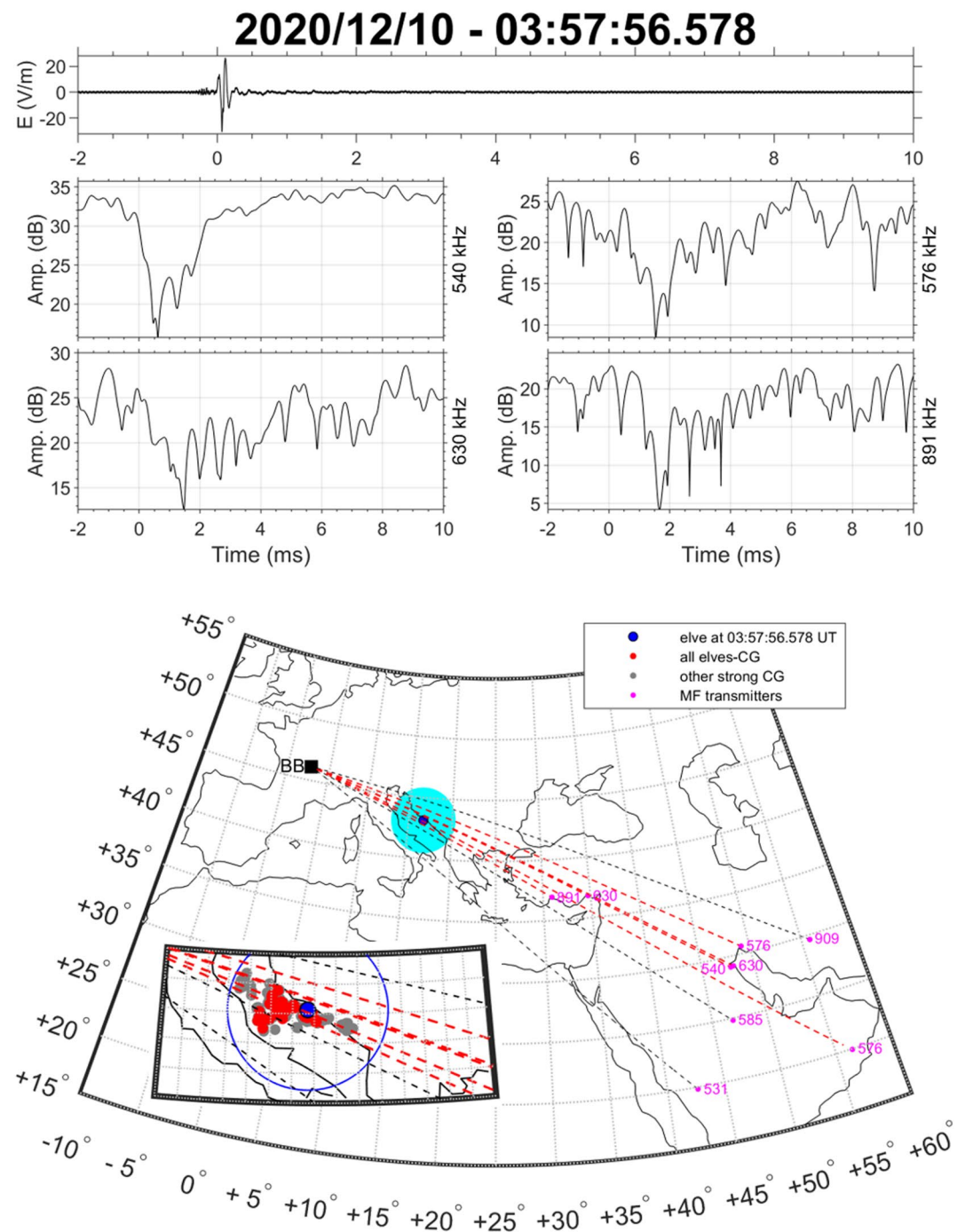


Figure 9. (top) Electric field associated with the elve observed at 03:57:56.578 UTC shown in Figure 2. The unit on the x-axis is ms. (middle): relative amplitude of four transmissions at 540, 576, 630 and 891 kHz (dB). (bottom): map showing the location of the strong CG strokes occurring during the 9–10 December 2020 over the Adriatic Sea (gray circles without elves, red ones with elves, the blue circle is for the elve at 03:57:56.578 UT and the light blue disk indicates where the elve is theoretically expanding), magenta dots show the location of transmitters used in this study and the dashed curves are the GCPs of each of these transmitters to the CEA station located in the center of France.

pronounced at 540 kHz, smaller for the three other frequencies and absent in the remaining three links. From the map, we see that the four links impacted pass close to the center of the elve. Other examples showing the seven MF narrowband signals, disturbed or not, are given in the Supporting Information (Figures S67–73 in Supporting Information S1).

The same technique used by Farges et al. (2007) was systematically employed here to calculate the parameters describing the perturbation. The peak attenuation, onset time, rise time and duration of the events were systematically measured after each CG stroke for the seven MF radio links, whether or not the MF perturbation was observed. The median, the mean and the standard deviation of these parameters are given for each transmitter in Table S3 of Supporting Information S1. These statistical values are also calculated, not taking into account the transmitter frequency, and are shown in Table 4 for the 59 events with elves and the 175 without and compared to the results from Farges et al. (2007).

Lightning affects MF-links in 86% of the 59 cases with elves, in line with Farges et al. (2007) for flashes over 60 kA, and in 53% of 175 cases without elves. We found that up to 5 MF-links can be disturbed with elves, but most often between 1 and 3. It is less likely that multiple links are perturbed simultaneously without elves. Perturbations are then observed more frequently with elves, and their presence seems to reflect an increase the size of the disruptive region. The number of MF-perturbations appears to depend on the local time of strokes without elves, whereas this trend is absent with elves (Figure S74 in Supporting Information S1).

Compared to the observations in Farges et al. (2007), the attenuation we observe is consistent with the ones predicted for CG peak currents higher than 125 kA. The onset times are shorter, the rise times (for elve cases) are similar, and the average duration is slightly shorter. According to Farges et al. (2007), such differences are to be expected. They note that the temporal parameters depend on the radio frequency and the relative locations of the stroke, transmitter, and receiver. The transmitter frequencies we use are lower (531–909 kHz vs. 900–1,557 kHz), and the links are longer (2540–5,650 km vs. 383–971 km). They find that the flash location relative to the link may affect the onset time up to a factor of ~ 3 . In addition, the CG strokes we consider are over the ocean, and those of Farges et al. (2007) are over land, which may affect the EMP in the lower ionosphere. We conclude, then, that the very brief MF radio emission perturbations are present even when the storm is between 882 and 1,330 km from the receiver. We also find from Table 4 that there is little difference in the parameters (except for MF attenuation occurrence) for events with elves and those with no elves. The lack of difference is perhaps because no-elves events do have elves that are undetected by the camera system. We have, indeed, cases without elves with E^2 of the same order of magnitude as with elves.

5. Discussion

The radio wave perturbations that were observed simultaneously with elves are the LOREs and the MF attenuations. We first discuss how they are related to elves, then continue with the early VLF events.

5.1. Elves, LOREs, and MF Attenuations

Our observations support the understanding that elves are associated with LOREs (Haldoupis et al., 2013), while the early VLF perturbations are distinct from LOREs and have other origins. However, 78% of the elves occur without LOREs and in the following we try to answer what determines the generation of a LORE.

As seen from Table 1, the presence of LOREs are not mirrored in the parameters derived from the ELF data. For instance, the CM is not significantly smaller for cases without LOREs. We cannot, then, search for an explanation in the ELF data. Turning to the VLF data, Marshall and Inan (2010) present a finite-difference, frequency domain model of narrow-band VLF transmitter signal propagation in the Earth-ionosphere wave-guide. They place an electron density perturbation at the ionospheric boundary at 85 km somewhere along the propagation path and calculate the changes in the signal properties at a receiver. They show that the amplitude perturbation can be both positive and negative, that it is largest if the disturbance is where the amplitude at the ground is low, such as an interference null, and can be suppressed entirely if it falls at an interference null at the reflection altitude. The amplitude also depends on parameters such as the path length, ionospheric and ground properties, and the signal frequency, however, the nighttime electron density fluctuations have a minor influence. In line with their model, we find both positive and negative perturbations in the amplitude and no dependence in local time of the occurrence of LOREs (see Figure 6a).

In Figure 8a, we show the location given by GLD360 of the CG strokes that produced elves and LOREs (early events are also shown), and in panel c a zoom of a region close to the VLF path. As noted earlier, Figure 8a shows that all negative LOREs come from the same storm and that the positive LOREs come from a different one. In that sense, the observations support the model results of Marshall and Inan (2010) and observations in

NaitAmor et al. (2013) that for a given TR-link the relative location of the lightning/disturbance and the VLF path is important for the sign of LOREs. The possible physical explanation for this is that the LORE signature is due to forward scattering or reflection from an area of perturbed conductivity to the receiver (Haldoupis et al., 2013; Rodger, 2003). The scattered or reflected signal beats with the direct signal to the receiver and, depending on their phase difference, there will be either constructive (positive LORE) or destructive (negative LORE) interference.

However, although many of the elves without LOREs are at a greater distance and different location relative to the VLF signal path, such as those of the cell at $\sim 42.8^\circ\text{N}$, $\sim 14.5^\circ\text{E}$, some are very close (Figure 8c). Since in this study, the ground and ionospheric conditions and the TR characteristics are the same for all elves, it suggests that other parameters related to the lightning and elves can affect the detection of LOREs. For example, we see from Figure 10a that elves with LOREs are brighter and produced by strokes of higher power and spectral energy, E^2 . This observation implies that the stroke energy should be large enough to create appreciable ionization before we can observe a LORE. Such a result could be anticipated based on the correlation between CG stroke peak current and LORE probability from Haldoupis et al. (2013) and that higher peak current strokes produce brighter elves (Barrington-Leigh & Inan, 1999) and larger electron density changes (Marshall et al., 2010). But observations showing the relationship between stroke peak current, broadband energy, elve brightness and LOREs has not been shown before.

The altitude of atmospheric perturbation may also affect the triggering of LOREs. Assuming that the main perturbation occurs where elves are generated, we see from Figure 10b that their altitudes are relatively high, from 86 to 90 km. This suggests that the altitude range of effective reflection and therefore the VLF frequency is important for the detection of LOREs. Still VLF propagation in the Earth-ionosphere waveguide is a complex physical process that depends non-linearly on several uncontrolled physical parameters and VLF transmitter signal characteristics such as irregular changes in the Earth-ionosphere waveguide, the scattering process itself, the phase difference at the receiver between the direct and the scattered signal, and so on. The interested reader can refer to Marshall and Inan (2010); Haldoupis et al. (2010); Gordillo-Vázquez et al. (2016) for more information. The present study cannot explain all the mechanisms behind the selective process of VLF event detection. This would require data from multiple sensitive VLF links cutting through the storm region in combination with modeling.

We next turn to the MF attenuations. Whereas changes in the D-region electron density cause LOREs, MF attenuation is related to the heating of electrons. Figure 10 show no simple relationship between MF attenuation and elve brightness, altitude, or lightning power. For example, lightning strokes with power $22\text{--}56\text{ (V/m)}^2$ generated elves with and without MF attenuations. The location of the disturbance relative to the signal path does, of course,

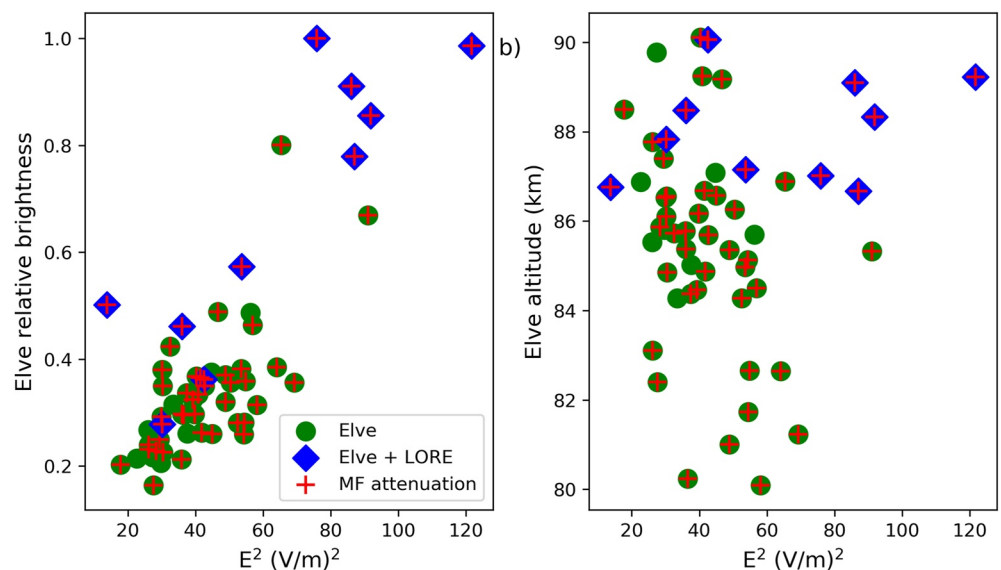


Figure 10. (a) Elve relative brightness versus stroke E^2 calculated over 1.5 ms. The elves associated with LOREs and MF attenuations are marked. (b) Elve altitude versus stroke E^2 calculated over 1.5 ms. The uncertainty on the altitude is ± 1.7 km.

play a role. However, in the region of Figure 8c, all but one observed elve created MF attenuations, which is the same proportion as overall.

Characterization and modeling of EMPs and their effect on the upper atmosphere is complicated, as is the modeling of wave propagation in the Earth-ionosphere waveguide and scattering and absorption of wave energy in D-region perturbations (Gordillo-Vázquez et al., 2016; Haldoupis et al., 2010; Marshall & Inan, 2010). We conclude that our dataset does not allow for understanding why some strokes trigger LOREs or MF attenuations and others do not, and that this requires further modeling and observations.

5.2. Early Events

Sprites are almost always associated with early VLF events, but early events may occur without the detection of sprites or any other type of luminous emissions, and it is not understood why (Haldoupis et al., 2010). However, it is clear that impulsive conductivity changes must be generated at ~70–80 km altitude with luminous emission that are either too dim to be detected (Pasko, 2010), or absent.

In the case of the storm we report on, no sprites or other luminous events were detected in relation to the early VLF events, although the camera horizon was below 70 km for 74% of the early events. Sprites are usually much brighter than elves when observed by video imaging cameras and should have triggered the camera. Nevertheless, one could argue that a storm that generates many elves and no sprites is uncommon and that the camera system, therefore, must have missed the sprites. However during the winter in Europe over sea in low CAPE conditions, storm cells do not develop large stratiform regions with positive charge reservoirs favorable for the +CG strokes that may trigger sprites. This was the case for the presented storm, where the storm cells were less than 100 km across. In addition, previous studies note that elves occur in Europe mainly over maritime thunderstorms, peaking from November to January, suggesting that the cold season thunderstorm charge configuration favors strokes with large EMPs (Arnone et al., 2020; Van der Velde & Montanyà, 2016). For these reasons it appears that the absence of detected sprites is not caused by problems with the camera system detection algorithm.

We find it more likely that optical emissions were too dim to be detected by the camera (dimmer than elves). One suggestion is that sprite streamers are stimulated, but do not reach luminosities sufficient to be detected as sprites (Haldoupis et al., 2010; Pasko, 2010). However data from two independent lightning detection systems agree that 12 of the 68 early events are caused by IC pulses. GLD finds 49 CG strokes, of these 21 +CG and 28 –CG. We are then left with strong indications that both IC pulses and CG strokes of both polarities generate early events. Since IC pulses and –CG strokes rarely generate sprites, it appears unlikely that undetected streamers cause the perturbations, unless, of course, these are quite common but rarely detected.

Another mechanism proposed relates to the halo. Halos are brief (few ms) unstructured layers of emissions at around 70–80 km altitude, which is at the upper end of sprite altitudes and the lower end of elves. They are centered above the causative lightning and extend 30–80 km horizontally (Barrington-Leigh & Inan, 2001; Wescott et al., 2001). It is suggested they are generated by the quasi-electrostatic and induction fields in the D-region ionosphere (Ren et al., 2019) following both polarities of CG lightning (Williams et al., 2007). They have to our knowledge not been observed for isolated IC discharges but are not well investigated because they generally appear dim in standard frame rate cameras, which makes them hard to detect (Inan et al., 2010). It is thought that halos represent increased ionisation, and that the field, therefore, is above the threshold field in an extended region mapped by optical emissions and beyond (Moore et al., 2003).

The electric field related to halos are thought to cause ionization, increasing the electron density and conductivity in a region where the field exceeds the threshold field, and to decrease the electron density in a layer below through electron attachment to neutral particles, driven by sub-break-down fields. This process increases the vertical conductivity gradient, with reduced absorption below and increased absorption above. The perturbation is proposed to lead to early VLF events, where their decay of 10–100 s is considered consistent with the lifetime of free electrons in the enhanced-density region at that altitude (Moore et al., 2003). It is further suggested that a larger diffuse region of perturbation on the scales of a few wavelengths of VLF transmitter signals better explain their scattering than the 100 m - 1 km scales of sprite structures (Inan et al., 2010).

A third proposed triggering mechanism for the observed early events are regions of electron density changes without optical emissions. Marshall et al. (2008) showed that density changes in the lower ionosphere by electron

Table 3
Charge Moment Change (CMC) for Discharges at the Time of Early Events

Event	Time (UTC)	Lon (deg)	Lat (deg)	Peak current (kA)	CMC (C km)
Early event a	23:17:50.311	16.75	42.94	-26	854.1
Early event a	23:17:50.616	16.71	42.91	+68	2708.8
Early event b	23:29:57.844	16.72	42.87	-210	818.2
Early event b	23:29:57.988	16.73	42.90	+19	2876.6
Early event c	23:41:10.851	16.76	42.88	+51	3535.2

Note. The lightning stroke parameters (GLD360) are only shown for the strongest discharges, although weaker discharges were also detected in most cases.

losses through dissociative attachment to molecular oxygen can create measurable amplitude changes in VLF transmitter signals that travel through the disturbed region. The energy required for attachment (3.7 eV) is lower than that of N₂ optical emissions often seen in sprites and elves (7.5 eV) and N₂ and O₂ ionization (15.6 eV) (Haldoupis et al., 2006; Neubert & Chanrion, 2013). This implies that attachment can occur without optical emission and ionization, explaining why we and other studies (e.g., Marshall et al., 2006) report early events without associated optical emissions, and also why optical emissions without early events are rare (Haldoupis et al., 2004, 2010). The timescales of recovery for density changes in the lower ionosphere controlled by attachment-detachment processes is in the order of 100 s (Pasko & Inan, 1994), consistent with the recovery times of the early events. As discussed in Marshall et al. (2008), a consequence of this hypothesis is that early VLF events caused by attachment-depleted regions would mostly have positive perturbation amplitudes due to less VLF signal absorption in the reduced density region. This scenario is consistent with our results as well as results from other previous studies (e.g., Haldoupis et al., 2004; Inan et al., 1993; Inan, Sampson, & Taranenko, 1996; Marshall et al., 2006).

Marshall et al. (2008) show that the field can be attributed to the EMP from successive IC lightning discharges. This is also suggested by observation reported in Johnson and Inan (2000) and Haldoupis et al. (2006) note that densely clustered EMPs of IC activity can explain the slower onset of early/slow events that do not match the timescales of return strokes. Model results from Gordillo-Vazquez et al. (2016) also showed that EMP effects on the ionosphere below 79 km by weak peak currents may produce attachment depleted regions that might be capable of generating early events. The cases we observe are related to positive and negative CG strokes, and IC pulses, and likely, both the EMP and the QE fields play a part. For example, the three cases summarized in Table 3 have ~500 ms sequences of flashes that reach relatively large CMCs that are well above the threshold for sprite production suggested in Cummer and Lyons (2005) and Yair et al. (2009) but likely increase too slowly for sprites or haloes to be observed (Hiraki & Fukunishi, 2006; Pasko et al., 1997). The observed sequences of flashes are similar to that of the sequential IC flashes assumed by Marshall et al. (2008) necessary to cause a cumulative effect of the attachment process so that an early fast event becomes strong enough to become detectable at the VLF receiver. Figure S65 in Supporting Information S1 shows the CM and CMC associated to the three early events in Table 3.

In summary, the observations of early events lead us to suggest that these observations may relate to regions of reduced conductivity caused by an electron attachment/detachment process at ~70 km altitude, or by electron enhancements associated with TLEs that are too dim to be detected by the camera.

6. Summary

We analyze for the first time observations of a large number of elves (63) from a single storm over the Adriatic Sea and associated perturbations to MF and VLF transmitter signals. We find two types of perturbations in the

Table 4
Statistics on MF Perturbation Characteristics When Elves Occur or Not (Attenuation Occurrence, Peak Attenuation, Onset Time, Rise Time and Duration): Mean, Standard Deviation (First Line of Each Cell in Columns 3–6) and Median (second Line)

	Occurrence	Peak attenuation (dB)	Onset time (ms)	Rise time (ms)	Duration (ms)
Elve	86%	-15.89 ± 5.27	0.98 ± 0.90	1.20 ± 0.80	3.48 ± 1.37
		16.19	0.96	1.03	3.34
No elve	53%	16.02 ± 5.70	0.68 ± 0.95	1.08 ± 0.76	3.25 ± 1.54
		15.89	0.62	0.90	3.06
Farges et al. (2007)	~90% for peak current > 60 kA	-8.34 ± 4.89	1.89 ± 0.73	1.25 ± 0.61	4.33 ± 1.59

Note. The previous study values are taken from Farges et al. (2007) for the 1,134 kHz radio link, which has the transmitter farthest from the receiver.

VLF transmitter signal: LOREs and early events. We also analyze the iCMC and CMC of selected lightning strokes. Based on the observations, we conclude that.

1. Several cases (14) of bright elves are found to be accompanied by LOREs, whereas many more elves (49) were detected without any concurrent VLF perturbations. The latter cannot be easily explained from the present data alone.
2. Our results suggest that bright elves at higher altitudes (>86 km), generated by high energy strokes are primarily associated with LOREs. This conclusion agrees with the understanding that bright elves relate to high peak current strokes.
3. The sign of the LORE depends on the location of the disturbance (elve) relative to the VLF TR path.
4. MF attenuations occur more often with elves (86%) than with CG strokes of similar high current, but without elves (53%).
5. From a subset of strokes, we find that CG strokes that produce elves have on average 3.2 times higher power, E^2 , in broadband and 3.1 times higher iCMC than strokes of similar peak current that do not produce observable elves.
6. We find that early events are associated with pure IC discharges and CG strokes of both polarities with no optical activity detected above the clouds, suggesting weak or no halo emissions from electric field-driven weak ionisation and/or electron attachment/detachment processes.
7. The three early events that were analyzed all correlated with lightning sequences with slowly increasing CMC (400–500 ms) that reached high values (>3,535 C km).

Data Availability Statement

The data used for this publication can be obtained from the public Zenodo repository: [10.5281/zenodo.6631859](https://doi.org/10.5281/zenodo.6631859). The GLD360 data are from 2020-12-09 19 UTC to 2020-12-10 06 UTC in the region lat: 36–45 N lon: 12.5–18 E. GLD data are proprietary and researchers may email brooke.pearson@vaisala.com to request GLD360 solution data. The ENTLN data used in this study were provided by Earth Networks. ENTLN data are proprietary but are freely available for scientific use by request at jeff.lapierre@aem.eco. We use the software 'Cartes du Ciel' version 2.76 (Chevalley, 2004) freely available for download at <https://www.ap-i.net/skychart/en/start>.

Acknowledgments

This study was made with the use of NSY transmitter data provided by R. Slošiar from the SOSA (Slovak Organization for Space Activities), Bratislava, Slovakia, and for this we are grateful. The authors thank Laboratoire Souterrain à Bas Bruit (LSBB), Rustrel, France, and its staff, for hosting our camera system. We also thank Vaisala and Ryan Said for providing GLD360 lightning data. In addition we thank Martin Füllekrug for interesting discussions on lightning waveforms. The authors thank the French AERIS/ICARE Data and Services Center which provided MSG/SEVIRI data for cloud top temperature. They also thank the European Copernicus/ECMWF Data Center, the US NCEP/NCAR and NOAA for providing meteorological reanalysis. The work of IK was supported by the GACR Grant 20-0967S. J. Mlynarczyk acknowledges support of the National Science Centre, Poland, under Grant 2015/19/B/ST10/01055.

References

- Arnone, E., Bór, J., Chanrion, O., Barta, V., Dietrich, S., Enell, C. F., et al. (2020). Climatology of transient luminous events and lightning observed above Europe and the Mediterranean Sea. *Surveys in Geophysics*, *41*(2), 167–199. <https://doi.org/10.1007/S10712-019-09573-5>
- Barrington-Leigh, C. P., & Inan, U. S. (1999). Elves triggered by positive and negative lightning discharges. *Geophysical Research Letters*, *26*(6), 683–686. <https://doi.org/10.1029/1999GL900059>
- Barrington-Leigh, C. P., Inan, U. S., & Stanley, M. (2001). Identification of sprites and elves with intensified video and broadband array photometry. *Journal of Geophysical Research*, *106*(A2), 1741–1750. <https://doi.org/10.1029/2000ja000073>
- Blaes, P. R., Marshall, R. A., & Inan, U. S. (2016). Global occurrence rate of elves and ionospheric heating due to cloud-to-ground lightning. *Journal of Geophysical Research A: Space Physics*, *121*(1), 699–712. <https://doi.org/10.1002/2015JA021916>
- Boeck, W. L., Vaughan, O. H., Blakeslee, R., Vonnegut, B., & Brook, M. (1992). Lightning induced brightening in the airglow layer. *Geophysical Research Letters*, *19*(2), 99–102. <https://doi.org/10.1029/91GL03168>
- Burgess, W. C. (1993). The role of ducted whistlers in the precipitation loss and equilibrium flux (p. 98).
- Carpenter, D. L., Inan, U. S., Trimpi, M. L., Helliwell, R. A., & Katsufakis, J. P. (1984). Perturbations of subionospheric LF and MF signals due to whistler-induced electron precipitation bursts. *Journal of Geophysical Research*, *89*(A11), 9857–9862. <https://doi.org/10.1029/JA089IA11P09857>
- Chang, S. C., Hsu, R. R., Huang, S. M., Su, H. T., Kuo, C. L., Chou, J. K., et al. (2014). Characteristics of TLE-producing lightning in a coastal thunderstorm. *Journal of Geophysical Research: Space Physics*, *119*(11), 9303–9320. <https://doi.org/10.1002/2014JA019819>
- Chang, S. C., Kuo, C. L., Lee, L. J., Chen, A. B., Su, H. T., Hsu, R. R., et al. (2010). ISUAL far-ultraviolet events, elves, and lightning current. *Journal of Geophysical Research*, *115*(A7), 0–46. <https://doi.org/10.1029/2009JA014861>
- Chen, A. B., Kuo, C.-L., Lee, Y.-J., Su, H.-T., Hsu, R.-R., Chern, J.-L., et al. (2008). Global distributions and occurrence rates of transient luminous events. *Journal of Geophysical Research*, *113*(A8), a–n. <https://doi.org/10.1029/2008JA013101>
- Chen, A. B., Su, H.-T., & Hsu, R.-R. (2014). Energetics and geographic distribution of elve-producing discharges. *JGR Space physics*, *119*(2), 1–1391. <https://doi.org/10.1002/2013JA019470>
- Chevalley, P. (2004). Cartes du Ciel, version 2.76. Retrieved from <https://www.ap-i.net/skychart/en/start>
- Cotts, B. R., & Inan, U. S. (2007). VLF observation of long ionospheric recovery events. *Geophysical Research Letters*, *34*(14), L14809. <https://doi.org/10.1029/2007GL030094>
- Cummer, S. A., & Lyons, W. A. (2004). Lightning charge moment changes in U.S. High plains thunderstorms. *Geophysical Research Letters*, *31*(5). <https://doi.org/10.1029/2003GL019043>

- Cummer, S. A., & Lyons, W. A. (2005). Implications of lightning charge moment changes for sprite initiation. *Journal of Geophysical Research*, *110*(A4), 4304. <https://doi.org/10.1029/2004JA010812>
- Davies, K. (1990). *Chap. 11: Ionospheric radio*. Peter Peregrinus.
- Farges, T., & Blanc, E. (2011). Champs électriques induits par les éclairs et les événements lumineux transitoires et leur effet sur l'ionosphère. *Comptes Rendus Physique*, *12*(2), 171–179. <https://doi.org/10.1016/j.crhy.2011.01.013>
- Farges, T., Blanc, E., & Tanguy, M. (2007). Experimental evidence of D region heating by lightning-induced electromagnetic pulses on MF radio links. *Journal of Geophysical Research*, *112*(A10), 10302. <https://doi.org/10.1029/2007JA012285>
- Frey, H. U., Mende, S. B., Cummer, S. A., Chen, A. B., Hsu, R. R., Su, H. T., et al. (2005). Beta-type stepped leader of elve-producing lightning. *Geophysical Research Letters*, *32*(13), 1–4. <https://doi.org/10.1029/2005GL023080>
- Fukunishi, H., Takahashi, Y., Sakanoi, K., Sakanoi, K., Inan, U. S., & Lyons, W. A. (1996). Elves: Lightning-induced transient luminous events in the lower ionosphere. *Geophysical Research Letters*, *23*(16), 2157–2160. <https://doi.org/10.1029/96gl01979>
- Gordillo-Vázquez, F. J., Luque, A., & Haldoupis, C. (2016). Upper D region chemical kinetic modeling of LORE relaxation times. *Journal of Geophysical Research: Space Physics*, *121*(4), 3525–3544. <https://doi.org/10.1002/2015JA021408>
- Haldoupis, C., Amvrosiadi, N., Cotts, B. R. T., Van der Velde, O. A., Chanrion, O., & Neubert, T. (2010). More evidence for a one-to-one correlation between Sprites and Early VLF perturbations. *Journal of Geophysical Research*, *115*(A7), 1–11. <https://doi.org/10.1029/2009ja015165>
- Haldoupis, C., Cohen, M., Arnone, E., Cotts, B., & Dietrich, S. (2013). The VLF fingerprint of elves: Step-like and long-recovery early VLF perturbations caused by powerful \pm cG lightning em pulses. *Journal of Geophysical Research: Space Physics*, *118*(8), 5392–5402. <https://doi.org/10.1002/jgra.50489>
- Haldoupis, C., Cohen, M., Cotts, B., Arnone, E., & Inan, U. (2012). Long-lasting D-region ionospheric modifications, caused by intense lightning in association with elve and sprite pairs. *Geophysical Research Letters*, *39*(16), 16801. <https://doi.org/10.1029/2012GL052765>
- Haldoupis, C., Mika, A., & Shalimov, S. (2009). Modeling the relaxation of early VLF perturbations associated with transient luminous events. *Journal of Geophysical Research*, *114*(A10). <https://doi.org/10.1029/2009JA014313>
- Haldoupis, C., Neubert, T., Inan, U. S., Mika, A., Allin, T. H., & Marshall, R. A. (2004). Subionospheric early VLF signal perturbations observed in one-to-one association with sprites. *Journal of Geophysical Research*, *109*(A10), 10303. <https://doi.org/10.1029/2004JA010651>
- Haldoupis, C., Steiner, R. J., Mika, A., Shalimov, S., Marshall, R. A., Inan, U. S., et al. (2006). Early/slow” events: A new category of VLF perturbations observed in relation with sprites. *Journal of Geophysical Research*, *111*(A11), A11321. <https://doi.org/10.1029/2006JA011960>
- Han, F., & Cummer, S. A. (2010). Midlatitude daytime D region ionosphere variations measured from radio atmospheric. *Journal of Geophysical Research*, *115*(A10), 10314. <https://doi.org/10.1029/2010ja015715>
- Han, F., Cummer, S. A., Li, J., & Lu, G. (2011). Daytime ionospheric D region sharpness derived from VLF radio atmospheric. *Journal of Geophysical Research*, *116*(A5), 5314. <https://doi.org/10.1029/2010ja016299>
- Hiraki, Y., & Fukunishi, H. (2006). Theoretical criterion of charge moment change by lightning for initiation of sprites. *Journal of Geophysical Research*, *111*(11), 1–6. <https://doi.org/10.1029/2006JA011729>
- Hunsucker, R. D. (1982). Atmospheric gravity waves generated in the high-latitude ionosphere: A review. *Reviews of Geophysics*, *20*(2), 293–315. <https://doi.org/10.1029/RG020I002P00293>
- Inan, U. S., Bell, T. F., Pasko, V. P., Sentman, D. D., Wescott, E. M., & Lyons, W. A. (1995). VLF signatures of ionospheric disturbances associated with sprites. *Geophysical Research Letters*, *22*(24), 3461–3464. <https://doi.org/10.1029/95GL03507>
- Inan, U. S., Cummer, S. A., & Marshall, R. A. (2010). A survey of ELF and VLF research on lightning-ionosphere interactions and causative discharges. *Journal of Geophysical Research*, *115*(6), 1. <https://doi.org/10.1029/2009JA014775>
- Inan, U. S., Pasko, V. P., & Bell, T. F. (1996). Sustained heating of the ionosphere above thunderstorms as evidenced in “early/fast” VLF events. *Geophysical Research Letters*, *23*(10), 1067–1070. <https://doi.org/10.1029/96GL01360>
- Inan, U. S., Rodriguez, J. V., & Idone, V. P. (1993). VLF signatures of lightning-induced heating and ionization of the nighttime D-region. *Geophysical Research Letters*, *20*(21), 2355–2358. <https://doi.org/10.1029/93GL02620>
- Inan, U. S., Sampson, W. A., & Tarantenko, Y. N. (1996). Space-time structure of optical flashes and ionization changes produced by lightning-EMP. *Geophysical Research Letters*, *23*(2), 133–136. <https://doi.org/10.1029/95GL03816>
- Johnson, M. P., & Inan, U. S. (2000). Sferic clusters associated with early/fast VLF events early/fast event association with. *Geophysical Research Letters*, *27*(9), 1391–1394. <https://doi.org/10.1029/1999gl010757>
- Kabirzadeh, R., Marshall, R. A., & Inan, U. S. (2017). Early/fast VLF events produced by the quiescent heating of the lower ionosphere by thunderstorms. *Journal of Geophysical Research: Atmospheres*, *122*(12), 6217–6230. <https://doi.org/10.1002/2017JD026528>
- Kolmašová, I., Santolík, O., Kašpar, P., Popek, M., Pizzuti, A., Spurný, P., et al. (2021). First observations of elves and their causative very strong lightning discharges in an unusual small-scale continental spring-time thunderstorm. *Journal of Geophysical Research: Atmospheres*, *126*(1), 1–23. <https://doi.org/10.1029/2020JD032825>
- Kumar, S., NaitAmor, S., Chanrion, O., & Neubert, T. (2017). Perturbations to the lower ionosphere by tropical cyclone Evan in the South Pacific Region. *Journal of Geophysical Research: Space Physics*, *122*(8), 8720–8732. <https://doi.org/10.1002/2017JA024023>
- Lapierre, J., Hoekzema, M., Stock, M., Merrill, C., & Thangaraj, S. C. (2019). Earth networks lightning network and dangerous thunderstorm alerts. *2019 11th Asia-Pacific International Conference on Lightning, APL 2019*. <https://doi.org/10.1109/APL.2019.8816032>
- Lu, G. (2006). 1 Transient electric field at high altitudes due to lightning: Possible role of induction field in the formation of elves. *Journal of Geophysical Research*, *111*(D2), 2103. <https://doi.org/10.1029/2005JD005781>
- Lu, G., Cummer, S. A., Blakeslee, R. J., Weiss, S., & Beasley, W. H. (2012). Lightning morphology and impulse charge moment change of high peak current negative strokes. *Journal of Geophysical Research*, *117*(4), 1. <https://doi.org/10.1029/2011JD016890>
- Mallik, S., Rakov, V. A., Hill, J. D., Ngin, T., Gamera, W. R., Pilkey, J. T., et al. (2014). Performance characteristics of the NLDN for return strokes and pulses superimposed on steady currents, based on rocket-triggered lightning data acquired. *Journal of Geophysical Research: Atmospheres*, *119*(7), 3825–3856. <https://doi.org/10.1002/2013JD021401>
- Marshall, R. A. (2012). An improved model of the lightning electromagnetic field interaction with the D-region ionosphere. *Journal of Geophysical Research*, *117*(3), 1. <https://doi.org/10.1029/2011JA017408>
- Marshall, R. A., & Inan, U. S. (2010). Two-dimensional frequency domain modeling of lightning EMP-induced perturbations to VLF transmitter signals. *Journal of Geophysical Research*, *115*(A6). <https://doi.org/10.1029/2009JA014761>
- Marshall, R. A., Inan, U. S., & Chevalier, T. W. (2008). Early VLF perturbations caused by lightning EMP-driven dissociative attachment. *Geophysical Research Letters*, *35*(21), L21807. <https://doi.org/10.1029/2008GL035358>
- Marshall, R. A., Inan, U. S., & Glukhov, V. S. (2010). Elves and associated electron density changes due to cloud-to-ground and in-cloud lightning discharges. *Journal of Geophysical Research*, *115*(A4). <https://doi.org/10.1029/2009JA014469>
- Marshall, R. A., Inan, U. S., & Lyons, W. A. (2006). On the association of early/fast very low frequency perturbations with sprites and rare examples of VLF backscatter. *Journal of Geophysical Research*, *111*(D19), 19108. <https://doi.org/10.1029/2006JD007219>

- Mika, A., Haldoupis, C., Neubert, T., Su, H. T., Hsu, R. R., Steiner, R. J., & Marshall, R. A. (2006). Early VLF perturbations observed in association with elves. *Annales Geophysicae*, 24(8), 2179–2189. <https://doi.org/10.5194/angeo-24-2179-2006>
- Mlynarczyk, J., Bór, J., Kulak, A., Popek, M., & Kubisz, J. (2015). An unusual sequence of sprites followed by a secondary TLE: An analysis of ELF radio measurements and optical observations. *Journal of Geophysical Research: Space Physics*, 120(3), 2241–2254. <https://doi.org/10.1002/2014JA020780>
- Moore, R. C., Barrington-Leigh, C. P., Inan, U. S., & Bell, T. F. (2003). Early/fast VLF events produced by electron density changes associated with sprite halos. *Journal of Geophysical Research*, 108(A10), 1363. <https://doi.org/10.1029/2002JA009816>
- NaitAmor, S., Cohen, M. B., Cotts, B. R., Ghalila, H., Alabdoadain, M. A., & Graf, K. (2013). Characteristics of long recovery early VLF events observed by the North African AWESOME Network. *Journal of Geophysical Research: Space Physics*, 118(8), 5215–5222. <https://doi.org/10.1002/jgra.50448>
- Neubert, T., & Chanrion, O. (2013). On the electric breakdown field of the mesosphere and the influence of electron detachment. *Geophysical Research Letters*, 40(10), 2373–2377. <https://doi.org/10.1002/grl.50433>
- Pasko, V. P. (2010). Recent advances in theory of transient luminous events. *Journal of Geophysical Research*, 115(6), 1. <https://doi.org/10.1029/2009JA014860>
- Pasko, V. P., & Inan, U. S. (1994). Recovery signatures of lightning-associated VLF perturbations as a measure of the lower ionosphere. *JGR Space physics*, 99(A9), 17523. <https://doi.org/10.1029/94JA01378>
- Pasko, V. P., Inan, U. S., Bell, T. F., & Taranenko, Y. N. (1997). Sprites produced by quasi-electrostatic heating and ionization in the lower ionosphere. *Journal of Geophysical Research*, 102(A3), 4529–4561. <https://doi.org/10.1029/96JA03528>
- Peter, W. B., & Inan, U. S. (2007). A quantitative comparison of lightning-induced electron precipitation and VLF signal perturbations. *Journal of Geophysical Research*, 112(12), 1. <https://doi.org/10.1029/2006JA012165>
- Poelman, D. R., Schulz, W., & Vergeiner, C. (2013). Performance characteristics of distinct lightning detection networks covering Belgium. *Journal of Atmospheric and Oceanic Technology*, 30(5), 942–951. <https://doi.org/10.1175/JTECH-D-12-00162.1>
- Qin, J., Celestin, S., & Pasko, V. P. (2013). Dependence of positive and negative sprite morphology on lightning characteristics and upper atmospheric ambient conditions. *Journal of Geophysical Research: Space Physics*, 118(5), 2623–2638. <https://doi.org/10.1029/2012JA017908>
- Ren, H., Tian, Y., Lu, G., Zhang, Y., Fan, Y., Jiang, R., et al. (2019). Examining the influence of current waveform on the lightning electromagnetic field at the altitude of halo formation. *Journal of Atmospheric and Solar-Terrestrial Physics*, 189(June), 114–122. <https://doi.org/10.1016/j.jastp.2019.04.010>
- Ripoll, J.-F., Farges, T., Malaspina, D. M., Cunningham, G. S., Lay, E. H., Hospodarsky, G. B., et al. (2021). Electromagnetic power of lightning superbolts from Earth to space. *Nature Communications*, 12(1), 3553. <https://doi.org/10.1038/s41467-021-23740-6>
- Rodger, C. J. (2003). Subionospheric VLF perturbations associated with lightning discharges. *Journal of Atmospheric and Solar-Terrestrial Physics*, 65(5), 591–606. [https://doi.org/10.1016/S1364-6826\(02\)00325-5](https://doi.org/10.1016/S1364-6826(02)00325-5)
- Rodger, C. J., Molchanov, O. A., & Thomson, N. R. (1998). Relaxation of transient ionization in the lower ionosphere. *Journal of Geophysical Research*, 103(A4), 6969–6975. <https://doi.org/10.1029/98JA00016>
- Said, R. K., Inan, U. S., & Cummins, K. L. (2010). Long-range lightning geolocation using a VLF radio atmospheric waveform bank. *Journal of Geophysical Research*, 115(23), 1–19. <https://doi.org/10.1029/2010JD013863>
- Said, R. K., & Murphy, M. J. (2016). GLD360 Upgrade: Performance analysis and Applications. *24th international lightning detection conference*. Salut, M. M., Abdullah, M., Graf, K. L., Cohen, M. B., Cotts, B. R., & Kumar, S. (2012). Long recovery VLF perturbations associated with lightning discharges. *Journal of Geophysical Research*, 117(8), 1–n. <https://doi.org/10.1029/2012JA017567>
- Van der Velde, O. A., & Montanya, J. (2016). Statistics and variability of the altitude of elves. *Geophysical Research Letters*, 43(10), 5467–5474. <https://doi.org/10.1002/2016GL068719>
- Wescott, E. M., Stenbaek-Nielsen, H. C., Sentman, D. D., Heavner, M. J., Moudry, D. R., & Sabbas, F. T. S. (2001). Triangulation of sprites, associated halos and their possible relation to causative lightning and micrometeors. *Journal of Geophysical Research*, 106(A6), 467–10477. <https://doi.org/10.1029/2000JA000182>
- Williams, E., Downes, E., Boldi, R., Lyons, W., & Heckman, S. (2007). Polarity asymmetry of sprite-producing lightning: A paradox? *Radio Science*, 42, RS2S17. <https://doi.org/10.1029/2006RS003488>
- Yair, Y., Price, C., Ganot, M., Greenberg, E., Yaniv, R., Ziv, B., et al. (2009). Optical observations of transient luminous events associated with winter thunderstorms near the coast of Israel. *Atmospheric Research*, 91(2–4), 529–537. <https://doi.org/10.1016/j.atmosres.2008.06.018>
- Zhu, Y., Stock, M., Lapierre, J., & Digangi, E. (2022). Upgrades of the Earth networks total lightning network in 2021. *Remote Sensing*, 14(9), 1–11. <https://doi.org/10.3390/rs14092209>